Materials Research Proceedings 28 (2023) 787-798 https://doi.org/10.21741/9781644902479-86

Damage prediction in roll forming of the high strength aluminum alloy AA7075

SUCKOW Timon[1,a *] and GROCHE Peter[1,b]

[1]Institute for Production Engineering and Forming Machines, TU Darmstadt, Otto-Berndt-Str. 2, 64287 Darmstadt, Germany

[a]suckow@ptu.tu-darmstadt.de, [b]groche@ptu.tu-darmstadt.de

Keywords: Roll Forming, Aluminum, 7075, Material Failure, Damage, FEM

Abstract. The high-strength AA7075 alloy offers great potential for lightweight construction thanks to its high specific strength. However, high strength and low ductility are challenging for forming the material in the peak-aged T6-condition in terms of material failure and springback. Therefore, this alloy is usually formed in temperature-supported process routes, which poses major challenges for process design. For cold forming of the alloy in the T6-condition, a reliable prediction of material failure is required in terms of process design. Within this study, this is achieved by applying the modified Mohr-Coulomb (MMC) criterion and an increment based damage evolution rule to the FE-model. To validate the failure prediction and verify the general applicability to different profile geometries, two U-profiles and a V-profile are roll formed. Failure occurs during forming for all profile geometries and the experimental results show a good agreement with the failure prediction. The quality of the damage prediction strongly depends on the calibration for the MMC criterion and the setup of the FE-model, depending on the mesh size and the element type used.

Introduction

Recent developments show that roll forming of high-strength aluminum alloys has become a focus of research and development [1-3]. Roll forming is an economical process for the production of long profiles, particularly in mass production [4]. For commercial vehicles, the use of high-strength aluminum is possible for the side impact beam, A- and B-pillars and other impact-absorbing components. The versatile shaping potential in roll forming compared to die or swivel bending processes allow additional design freedom for the optimal design of the profiles [5]. Additionally, smaller bending radii can be achieved during roll forming, which contributes to an increase in design freedom [6,7].

However, high strength and low ductility of lightweight materials, such as the AA7075 alloy, are challenging for process design. This is expressed in large safety factors and compromises in terms of the target geometry of components, especially with regard to achievable bending radii and bending angles. Process design is of particular relevance in roll forming due to the three-dimensional forming, as various production-related defects can occur. In roll forming of high-strength materials, the occurrence of cracks in the outer fibre of the bending zone and a high springback are critical [8]. The occurrence of cracks is particularly critical for small ratios of the bending radius r to the sheet thickness s and for large bending angles. A plane strain state is present in the outer fibre of the bending zone where fracture occurs [9].

Damage Prediction. Accurate prediction of damage is necessary to improve process design. The modelling of damage in forming technology has been developed over the last decades and is used in the design of forming processes for the optimal utilisation of process windows and for the prediction of material failure [10]. Failure is the final stage of damage and appears in forming processes through intolerable and function-restricting cracks [11]. In general, the damage of metals can be described using uncoupled fracture criteria or coupled damage models [11]. In coupled

damage models, the elastic and/or plastic material behaviour is linked to the evolution of damage. Due to the higher practicability, uncoupled fracture criteria are widespread in the field of metal forming [11]. Metals usually fail as the result of nucleation, growth and coalescence of microscopic voids within the metal structure during forming processes [12]. All three mechanisms are dependent on the stresses and strains during forming. Developments in modelling damage have shown that damage is dependent on the stress triaxiality η [12,13]. The stress triaxiality η is defined as the ratio of the hydrostatic stress σ_m to the equivalent stress $\bar{\sigma}$:

$$\eta = \frac{\sigma_m}{\bar{\sigma}} \tag{1}$$

where hydrostatic stress,

$$\sigma_m = \frac{\sigma_1+\sigma_2+\sigma_3}{3} \tag{2}$$

equivalent stress,

$$\bar{\sigma} = \sqrt{\frac{(\sigma_1-\sigma_2)^2+(\sigma_2-\sigma_3)^2+(\sigma_3-\sigma_1)^2}{2}} \tag{3}$$

and σ_1, σ_2 and σ_3 are the principal stresses. Another significant parameter for the extent of damage in three-dimensional stress states is the Lode angle parameter $\bar{\theta}$. This is relevant especially for small stress triaxialities and is employed for example in the modified Mohr-Coulomb (MMC) criterion by Bai and Wierzbicki [13] and the Lou-Huh criterion [12]. All stress directions (loading conditions) can be characterized by the parameters η and $\bar{\theta}$,.

MMC Criterion. The equivalent plastic strain at fracture $\bar{\varepsilon}_f$ depends on the stress triaxiality and the lode angle parameter in the MMC criterion [14]:

$$\bar{\varepsilon}_f = \left\{\frac{A}{c_2}[1-c_\eta(\eta-\eta_0)] \times \left[c_\theta^s + \frac{\sqrt{3}}{2-\sqrt{3}}(c_\theta^{ax}-c_\theta^s)\left(\sec\left(\frac{\bar{\theta}\pi}{6}\right)-1\right)\right]\left[\sqrt{\frac{1+c_1^2}{3}}\cos\left(\frac{\bar{\theta}\pi}{6}\right)+c_1\left(\eta+\frac{1}{3}\sin\left(\frac{\bar{\theta}\pi}{6}\right)\right)\right]\right\}^{-\frac{1}{n}} \tag{4}$$

Eight parameters (A, n, c_η, η_0, c_θ^s, c_θ^{ax}, c_1 and c_2) need to be found for the calibration of the MMC criterion, but only two have to be determined from fracture tests. An explanation of the parameters can be found in [14]. The effects of c_η and c_1 are similar in terms of stress triaxiality, which reduces Eq. 4 to:

$$\bar{\varepsilon}_f = \left\{\frac{A}{c_2}\left[c_\theta^s + \frac{\sqrt{3}}{2-\sqrt{3}}(c_\theta^{ax}-c_\theta^s)\left(\sec\left(\frac{\bar{\theta}\pi}{6}\right)-1\right)\right]\left[\sqrt{\frac{1+c_1^2}{3}}\cos\left(\frac{\bar{\theta}\pi}{6}\right)+c_1\left(\eta+\frac{1}{3}\sin\left(\frac{\bar{\theta}\pi}{6}\right)\right)\right]\right\}^{-\frac{1}{n}} \tag{5}$$

The parameters A and n are determined from the power hardening curve: $\bar{\sigma} = A\varepsilon^n$ [14]. The parameters c_1 and c_2 are determined from material tests up to material fracture, where the fracture strain $\bar{\varepsilon}_f$, stress triaxiality η and lode angle parameter $\bar{\theta}$ are determined numerically and/or experimentally. For accurate damage prediction, the tests should cover load paths that are close to the investigated forming process [11]. The parameters c_θ^{ax} and c_θ^s could be determined from careful plasticity tests and determination of the yield surface [14]. Potential simplifications are the assumption of c_θ^{ax}=1 and $c_\theta^s = 1$ or the determination of the values by the material tests up to

Materials Research Proceedings 28 (2023) 787-798 https://doi.org/10.21741/9781644902479-86

fracture [14]. The final function provides a three-dimensional fracture locus in the space of stress triaxiality and lode angle parameter. A relationship between the equivalent plastic strain $\bar{\varepsilon}_p$ during the forming process and the equivalent plastic strain at fracture $\bar{\varepsilon}_f = f(\eta, \bar{\theta})$ from the fracture locus provides the damage evolution rule, where material failure occurs when $D \geq 1$ [13]:

$$D(\bar{\varepsilon}_p) = \int_0^{\bar{\varepsilon}_p} \frac{d\bar{\varepsilon}_p}{f(\eta,\bar{\theta})} \tag{6}$$

Damage Prediction in Roll Forming. Wang et al. [15] provide an example for the application of damage models in roll forming with the application of the Oyane model. Shear stresses in the forming zone are responsible for material failure [15]. Furthermore, Wang et al. [15] hypothesize that roll forming seems to be a sheet forming process but is intrinsically a bulk forming process in terms of stress and strain state. Deole et al. [8] use the fracture criterion of Lou and Huh [16] for failure prediction. For calibration, additional bending tests are carried out to represent the plane strain state over the entire loading path [8]. In contrast to [15], the damage and final material failure are related to the plane strain tension state in the outer edge fibre in the bending radius [8]. In the work of Talebi et al. [9], fracture criteria (Rice-Tracey, Crockoft-Latham and Ayada) are used with two different approaches to calibrate the models. The basic approach is the calibration of the model with a uniaxial tensile test. In the extended calibration, with additional material tests, the failure prediction error is reduced from 88 % to 8 % [9]. Lee et al. [2] provide another study on fracture and damage modelling on the roll forming of a bumper beam made of the high-strength aluminum alloy AA7075-T6 using the GISSMO damage model. The summary of the previous approaches shows contradictory statements on the dominant failure-critical stress states and emphasizes the relevance of the calibration and application of fracture criteria and damage models in roll forming. All approaches have in common, that only one profile flower is investigated. Within this study, three different profile flowers are investigated. Due to the application-oriented research, an industrially widespread FE-solver (Marc Mentat) for roll forming is used for the numerical simulation, as well as for calibration of the MMC criterion. All tests for calibration of the MMC criterion are conducted on a universal testing machine. The aim of the study is to apply an easy-to-use fracture criterion in combination with a damage evolution rule on the one hand. On the other hand, a low experimental and numerical effort with a simultaneously accurate damage and failure prediction is strived for.

Results

Calibration of the MMC Criterion. To calibrate the MMC criterion for the peak-aged AA7075-T6 alloy, material tests up to fracture are performed on a Zwick Roell 100 universal testing machine for measuring the equivalent plastic strain at fracture $\bar{\varepsilon}_f$. Plastic strain is measured by optical strain measurement with the GOM Aramis system, after applying a stochastic pattern on the surface of the specimens. Three specimens were tested for each geometry. Before testing, the specimens were milled out of the sheet metal at a 90 ° angle to the rolling direction. Additionally, FE-simulations of the material tests are carried out for each geometry in Marc Mentat 2012 for determining the average values of the stress triaxiality η_{avg} and the lode angle parameter $\bar{\theta}_{avg}$ during plastic deformation. Within the material tests, different loading conditions in terms of stress triaxiality and lode angle parameter are applied. Fig. 1a shows the strain paths for different specimens and

the parameter set, obtained by the material tests and Fig. 1b shows the specimens for calibration of the MMC criterion.

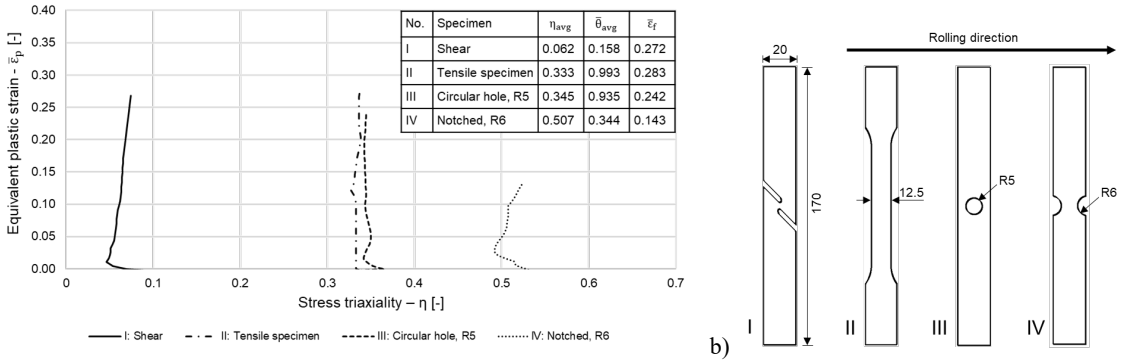

Fig. 1. a) Plastic strain $\boldsymbol{\varepsilon_f}$ and stress triaxiality $\boldsymbol{\eta}$ during the calibration experiments. b) Specimens for calibration of the MMC criterion: I: Shear; II: Tensile specimen; III: Circular hole, R5; IV: Notched, R6.

The set of parameters is the basis for calculating the constants of the MMC criterion. Since the lode angle parameter $\bar{\theta}$ is greater than zero for all specimens, c_θ^{ax} is set to 1, as recommended by Bai and Wierzbicki [14]. The remaining parameters c_1, c_2 and c_θ^s are determined by the nonlinear least-squares solver "lsqcurvefit" via Matlab:

$$\min_{(c_1,c_2,c_\theta^s)} (\Delta\bar{\varepsilon}_f)^2 = \min_{(c_1,c_2,c_\theta^s)} \left[\frac{1}{N}\sum_{i=1}^{N}\left(\bar{\varepsilon}_{f,i} - \hat{\bar{\varepsilon}}_{f,i}(c_1,c_2,c_\theta^s)\right)^2\right] \tag{7}$$

The values for $\bar{\varepsilon}_{f,i}$ are determined from the calibration tests, while $\hat{\bar{\varepsilon}}_{f,i}(c_1,c_2,c_\theta^s)$ are the function values of the optimized MMC criterion (Eq. 5). The parameters $n = 0.0862$ (hardening exponent) and $A = 784.96$ are obtained from the flow curve from uniaxial tensile tests. In addition, the tensile strength $R_m = 590$ MPa and yield strength $R_{p0,2} = 528$ MPa are determined in these tests. Fig. 2a shows the calibrated fracture locus in the $(\eta, \bar{\theta}, \bar{\varepsilon})$-space and Fig. 2b in the $(\eta, \bar{\varepsilon})$-space.

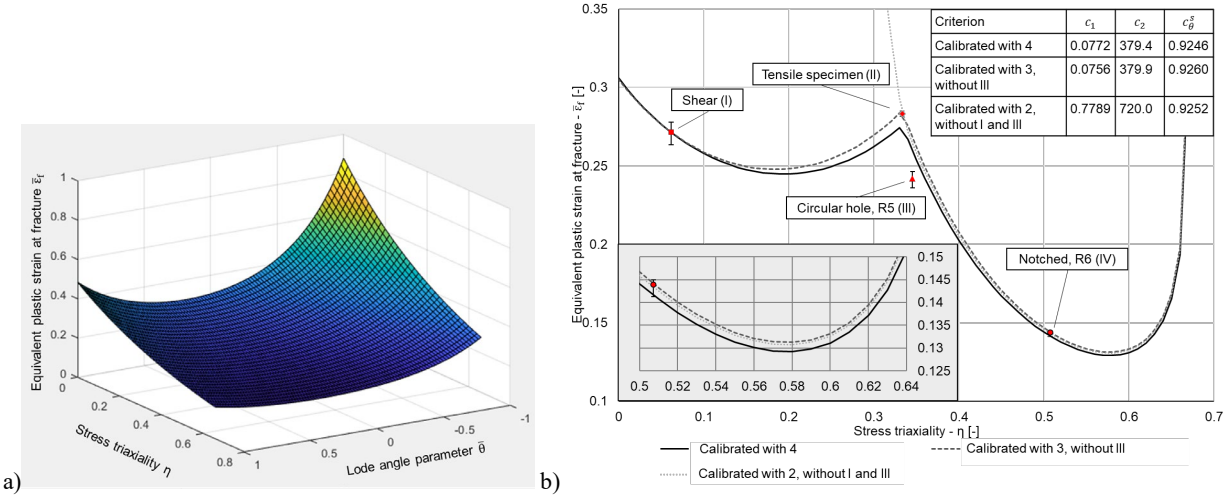

Fig. 2. Representation of the MMC fracture criterion. a) In the $(\boldsymbol{\eta}, \boldsymbol{\bar{\theta}}, \boldsymbol{\bar{\varepsilon}})$-space, calibrated with 4 specimens. b) In the $(\boldsymbol{\eta}, \boldsymbol{\bar{\varepsilon}})$-space for plane stress condition. Calibrated with 2, 3 and 4 specimens.

Materials Research Proceedings 28 (2023) 787-798 https://doi.org/10.21741/9781644902479-86

To investigate the influence of various specimen geometries on the shape of the fracture locus, the fracture locus is illustrated in $(\eta, \bar{\varepsilon})$-space, which is representative for plane stress condition. In plane stress condition, η and $\bar{\theta}$ are dependent on each other, as shown in Eq. 8:

$$\bar{\theta} = 1 - \frac{2}{\pi} \cdot \cos^{-1}\left(-\frac{27}{2}\eta\left(\eta^2 - \frac{1}{3}\right)\right) \tag{8}$$

The shape of the fracture locus is influenced by removing material tests for calibration of the fracture locus (Fig. 2b). Calibrating the fracture criterion with two, three, four or five specimens does not have a high impact on the shape of the fracture locus for stress triaxialities above $\eta = 0.\overline{3}$. During roll forming, bending stresses are expected to be dominant during forming. This would correspond to a stress triaxiality of $\eta = 0.577$. The max. relative error of the fracture locus in plane stress condition for the stress triaxiality of $\eta = 0.577$ is 1.1 % ($\bar{\varepsilon}_f = 0.0014$). For the stress triaxiality of $\eta = 0.\overline{3}$, the relative error is 3.3 % ($\bar{\varepsilon}_f = 0.009$). Less material tests for the calibration of the MMC criterion result in reduced experimental effort and thus in a more efficient calibration of the criterion. The effect of a reduced number of material tests on the damage prediction during roll forming is discussed within this study.

Experimental Setup. Within this study, three different profiles are investigated in order to apply different loading conditions in the bending zone, as shown in Fig. 3a. The profile flowers are presented in each case up to the stage where failure occurs. The difference between the U-profiles is the forming strategy (constant radius vs. constant length) and the flange length. The experiments were performed on two different roll forming machines. The U-profiles were formed on a VOEST P 450/4 roll forming machine and the V-profile on another conventional roll forming machine of the Deakin University, Australia. Feeding speed of the sheet was 1 m/min, the initial sheet length 1500 mm and no lubrication was used. Within the roll forming experiments, the cracks occurred in the bending radii for all profile flowers. Fig. 3b shows the experimental setup for roll forming of a U-Profile and the occurrence of cracks after the third pass.

a)

U-Profile - constant radius		
Interstation distance: 520 mm		
Roll diameter: 250 mm		
Initial sheet width: 170 mm		
Flange length: 42.5 mm		
Pass	Angle [°]	Radius [mm]
1	13	3
2	29	3
3	47	3

U-Profile - constant length		
Interstation distance: 520 mm		
Roll diameter: 250 mm		
Initial sheet width: 170 mm		
Flange length: 57.2 mm		
Pass	Angle [°]	Radius [mm]
1	15	17,004
2	30	8,049
3	45	5,096

V-Profile - constant length		
Interstation distance: 400 mm		
Roll diameter: 140 mm		
Initial sheet width: 75 mm		
Pass	Angle [°]	Radius [mm]
1	10	25,85
2	20	12,6
3	30	8,18
4	40	5,98
5	50	4,65
6	60	3,77

b)

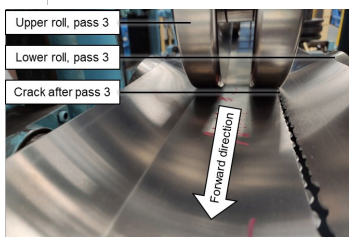

Fig. 3. Profile flowers, investigated within this study. Fracture occurred in the last pass for each profile within the roll forming experiments (marked red).b) Experimental setup and occurrence of cracks (U-Profile - constant radius).

FE Model. The aim of the FE model is to support the design of the roll forming process with regard to the final geometry and manufacturing-related defects such as material failure. By applying the MMC criterion in combination with a damage evolution rule in the FE model, a prediction of the damage and thus a determination of the process limits is possible. Accurate prediction of damage requires accurate prediction of local stresses and strains in the FE model. The setup of the FE model including material parameters and boundary conditions is shown in Fig. 4. Mesh size and element type are varied with regard to the conflict of objectives between a good prediction of the stresses and strains and the computation time. The variation of the mesh size is similar for all profiles. The mesh size in the bending zone is small, compared to the remaining part of the sheet. The flow curve is obtained from uniaxial tensile tests with a strain rate of 0.002 1/s.

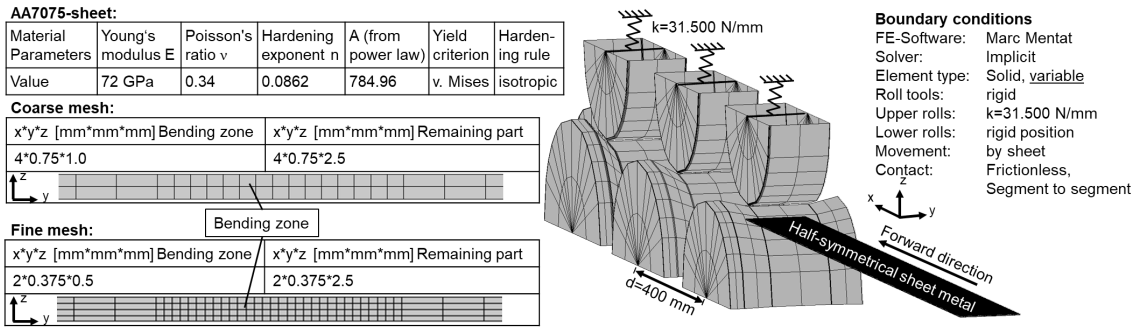

Fig. 4. Setup of the FE model based on the example of the U-profile (constant radius).

Damage Prediction. For damage prediction, the MMC-criterion is applied to the critical node in the FE-model, which is on the outer fibre of the bending zone. Fig. 5a shows the evaluation node for investigating the roll forming process and damage prediction within this study. For all profile flowers, the node is located at the point with the highest plastic strain in the failure-critical forming stage. The node is located in the steady-state area of the sheet at a length of 600 mm (half sheet length). Plastic deformation in the bending zone occurs primarily, when the sheet passes through the forming rolls (Fig. 5b). The stress exceeds the yield stress, which leads to a permanent plastic deformation.

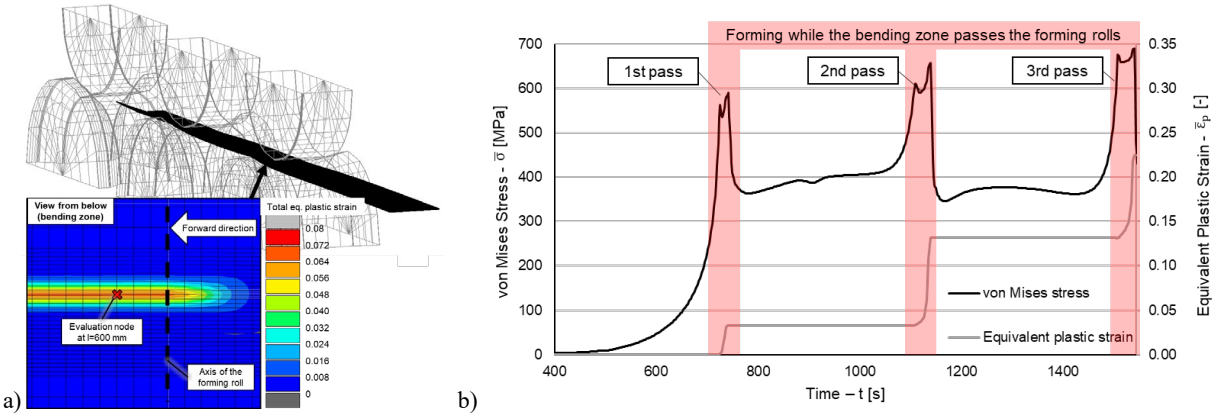

Fig. 5. a) Location of the evaluation node in the bending zone in the example of the U-profile (constant radius). b) Development of equivalent plastic strain and von Mises stress during the roll forming process.

For nonlinear loading paths, a nonlinear incremental rule must be applied for accurate prediction of damage, as proposed by Bai and Wierzbicki [13]. Within this study, the loading path is considered in the damage evolution rule by summing up the damage value for each increment in the FE-simulation, while considering the loading condition in terms of stress triaxiality and lode angle parameter. For an accurate prediction of damage, the time step for each increment should be small enough to represent the current stress- and strain state and thus the loading path during forming. In this study, one increment is evaluated every 2 mm in the forward direction of the sheet. Increasing the distance to 10 mm per increment leads to a relative error in damage prediction of up to 15 %, due to the inaccurate representation of the loading path. The incremental damage D_{inc} for each node and time increment in the FE-model is calculated by the following equation:

$$D_{inc,\ t} = \frac{\bar{\varepsilon}_{p,t} - \bar{\varepsilon}_{p,t-1}}{\frac{1}{2}\left(\bar{\varepsilon}_f(\eta,\bar{\theta})_t + \bar{\varepsilon}_f(\eta,\bar{\theta})_{t-1}\right)} \tag{9}$$

where $\bar{\varepsilon}_{p,t}$ is the equivalent plastic strain at the evaluated node in the FE-model and $\bar{\varepsilon}_f(\eta,\bar{\theta})_t$ is the equivalent strain at fracture, calculated by the loading condition $(\eta,\bar{\theta})$ of the evaluation node. The total Damage D is defined as the sum of the incremental damage D_{inc}, where n is the total number of increments up to the evaluated time t in the FE-model:

$$D = \sum_{t=1}^{n} D_{inc,t} \tag{10}$$

In the following section, the damage prediction is applied for different profile flowers, mesh and element types. Table 1 shows the naming scheme for the FE-models. Fig. 6 depicts the loading condition for the different profile flowers in order to analyze the differences between the different profile types. The stress states correspond to the plane-stress state and the calibration tests cover a large section of the load path, but the difference between the profile flowers is small. Furthermore, for all profile flowers, the non-linear loading paths follow a similar trend, with increasing stress triaxiality during bending in roll forming in each pass. At the beginning of the plastic deformation in each stage, the loading condition is between shear and uniaxial tension and develops towards stress states between plane strain tension and biaxial tension. An additional test for matching the biaxial tension would be helpful to cover all loading conditions, but is not possible with a universal testing machine.

Table 1. Naming scheme for the FE-models.

Profile	**Mesh**	**Element type**
U-cR: U - constant radius	**C**: coarse	**FI**: Fully integrated 8-node-Element (Type 7)
U-cL: U - constant length	**F**: fine	**RI**: 8-node Element with reduced integration / hourglass control (Type 117)
V: V-Profile		

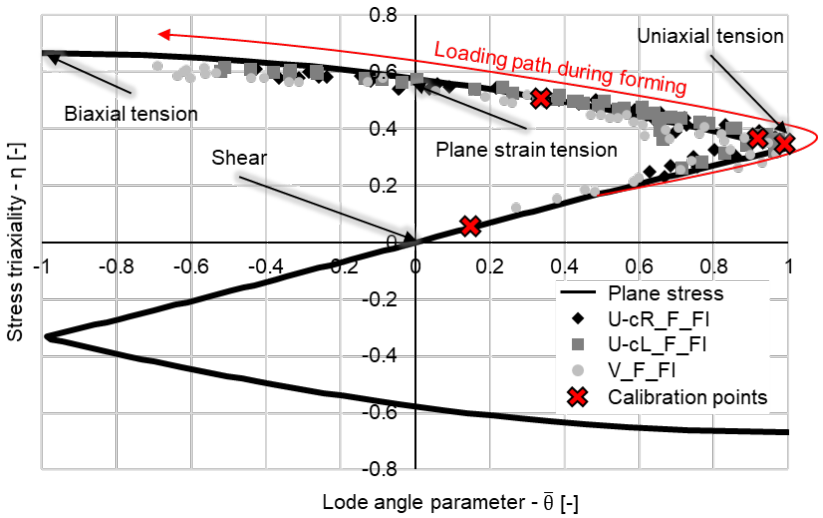

Fig. 6. Representation of the loading condition during plastic forming in the outer fibre of the bending zone for different profile flowers compared to the plane stress condition and the calibration tests.

After a short introduction to the typical stress states during roll forming, various parameters in the FE models are analyzed. The aim is an accurate and efficient prediction of the damage. Efficient means with low experimental and numerical effort. If it is not explicitly described, the prediction of the damage is based on the MMC criterion, based on four material tests. Table 2 and Fig. 7 show the results for different profile flowers, varying the element type and the mesh size in order to overcome the conflict of objectives. It is shown, that the damage is underestimated when the mesh is too coarse, which is fatal for a process design. The same tendency is shown for the reduced integrated elements. This is mainly due to the underestimated plastic strain and stress triaxiality. For the V-profile, the trend is reversed, although the differences are significantly smaller. Furthermore, this leads to a conservative process design and is therefore not too critical. In summary, the fully integrated elements with fine meshing provide the best results in terms of damage prediction. However, the computation time is high, particularly for the fine meshed simulations: 55.200 elements (153 h) instead of 10.800 elements (16 h) for the coarse mesh. The reduced integrated elements decrease the computation time by approx. 5 %. Finer meshing is not practicable due to the already high computing time.

*Table 2. Comparison of ductile fracture (experimental) and predicted damage (numerical) for different mesh and element types. Damage underestimated numerically: marked in red. *Fracture estimated in pass 5 already.*

Profile flower	**U-Profile (constant radius)**				**U-Profile (constant length)**				**V-Profile**			
Mesh	C		F		C		F		C		F	
El. Type	FI	RI	FI	RI	FI	RI	FI	RI	FI	RI	FI	RI
Ductile fracture (exp.)	3rd pass				3rd pass				6th pass			
Damage at pass of experimental fracture	1.08	0.96	1.52	1.42	0.91	0.75	1.01	0.99	1.16	1.19	1.03*	1.09

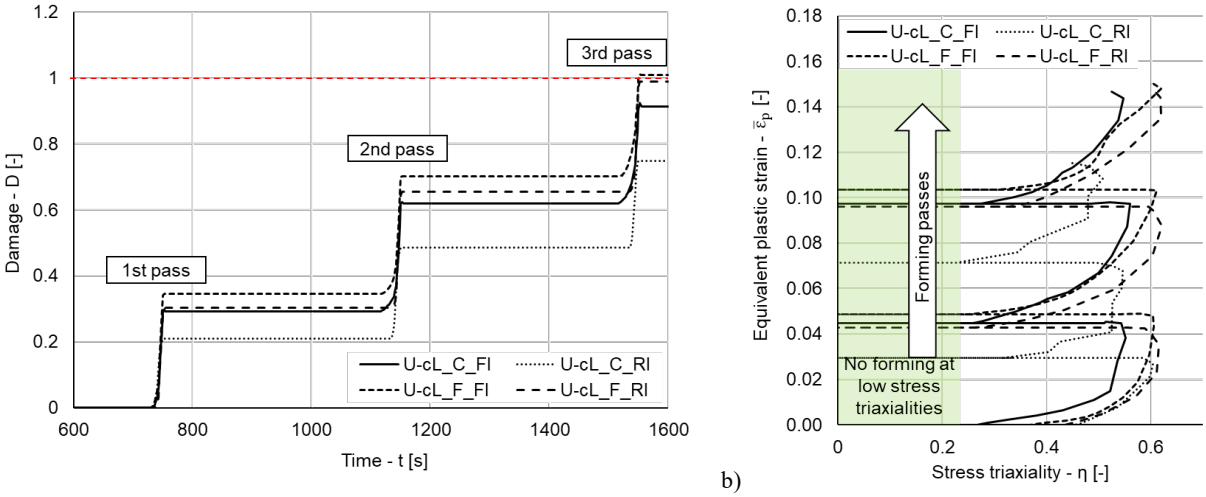

Fig. 7. Numerical prediction of damage (a) and loading paths (b) in the $(\boldsymbol{\eta}, \bar{\boldsymbol{\varepsilon}})$-space during roll forming of the U-Profile (constant length), for different mesh sizes and element types.

In Fig. 8, the different profile types are compared to each other in terms of damage prediction with the best-suited mesh and element type: fully integrated elements with a fine mesh. Damage prediction for the U-Profiles is accurate, while material failure for the V-Profile is predicted too early. Damage is 1.03 in pass 5 already, although there is no material failure experimentally until the 6th pass. This corresponds to an error in the damage prediction of at least 3 %.

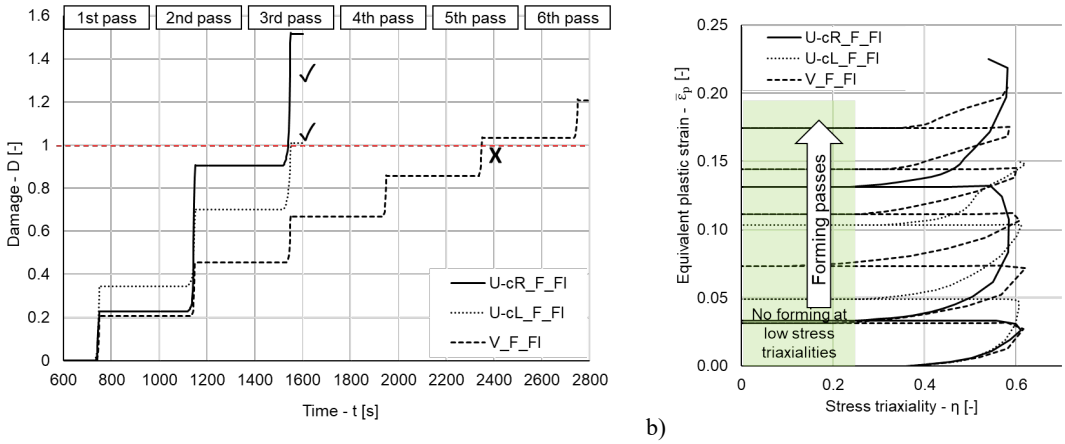

Fig. 8. Numerical prediction of damage (a) and loading paths (b) in the $(\boldsymbol{\eta}, \bar{\boldsymbol{\varepsilon}})$-space during roll forming for all profiles.

In the following section, the MMC criteria, calibrated with a varying number of material tests (Fig. 2b), are compared in terms of failure prediction. Table 3 and Fig. 9 show the results in relation to the number of material tests for calibration of the MMC criterion. Excluding material tests to calibrate the MMC criterion leads to a less accurate prediction of damage. In this case, the damage is underestimated. The reason is the insufficiently represented loading condition in the calibrated MMC criterion, which is replaced by model-based assumptions. The exclusion of a single sample (III: circular hole) leads to a small but decisive deviation in the damage prediction for the U-profile (constant length). The additional exclusion of the shear specimen (I), however, leads to a high deviation of the damage prediction of up to 16 %. This highlights the fact that not only the plane strain condition should be captured to calibrate the damage criterion, as further loading conditions, even $\eta < 0.33$, occur during roll forming.

*Table 3. Comparison of ductile fracture (experimental) and predicted damage (numerical) for different calibrations. Damage underestimated numerically: marked in red. *Fracture estimated in pass 5 already.*

Profile flower	**U-Profile (constant radius)**			**U-Profile (constant length)**			**V-Profile**		
Calibrated with X material tests	4	3	2	4	3	2	4	3	2
Damage at pass of experimental fracture	1.52	1.49	1.31	1.01	0.99	0.96	1.03*	1.01*	0.95

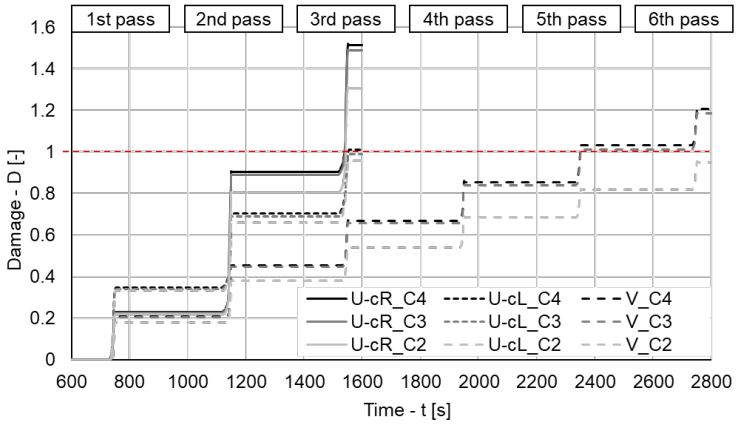

Fig. 9. Numerical prediction of damage for different calibrations of the MMC criterion.

Summary

The investigations have shown that roll forming of the high-strength aluminum alloy AA7075 in the peak-aged T6-condition is challenging, as material failure occurs in an early stage of the process. The application of the MMC criterion in combination with the used incremental damage evolution rule is suitable for predicting material failure during roll forming of the AA7075 alloy. This is even possible for a simple setup of the FE-model, with a von Mises yield criterion, an isotropic hardening rule and neglecting the friction. The roll forming process covers a wide range of loading conditions in terms of stress triaxiality η and Lode angle parameter $\bar{\theta}$, independent of the profile flower. The loading paths are not linear, as they include loading conditions from shear/uniaxial tension up to plane strain tension and biaxial tension, but the used incremental damage evolution rule was shown to be suitable for damage and failure prediction.

The calibration of the MMC criterion is based on material tests with optical strain measurement for determining fracture strain $\bar{\varepsilon}_f$ and FE-simulations for determining the stress triaxiality and the Lode angle parameter. The FE solver Marc Mentat proved to be suitable for performing the material tests and the roll forming simulation. For calibration of the MMC criterion it is recommended to use at least a tensile specimen, a notched specimen and a shear specimen. Otherwise, the loading conditions occurring during roll forming are only insufficiently represented in the MMC criterion. Adding a specimen with a circular hole leads to further improvement of damage prediction. Another result of the study is the recommendation of the element type and meshing that is best suited for predicting the damage. A prediction of the global material behavior, e.g. the forming force or springback is given with a coarse mesh [1]. However, for accurate prediction of damage, the prediction of local stresses and strains must also be accurate, but too fine meshing results in excessive computation time. Therefore, a meshing with four elements in thickness direction with fully integrated elements is recommended.

The inaccurate damage prediction for the V-profile may be due to the high non-linearity of the loading path compared to the other profile flowers. Given that the tests were carried out with one

material, further tests should be carried out with different materials to confirm the suitability of the MMC criterion in combination with the incremental damage evolution rule used.

Acknowledgement
The authors gratefully acknowledge financial support from the Hessen State Ministry for Higher Education, Research and the Arts- Initiative for the Development of Scientific and Economic Excellence (LOEWE) for the Project ALLEGRO (Subproject A1). In addition, the authors would like to thank the DAAD for funding the international exchange programme "Laser heat assisted roll forming of new high strength aluminium alloys" and the Institute for Frontier Materials at Deakin University for the support in conducting the roll forming tests (V-profile) within this project. Further thanks go to my colleague Dirk Molitor for programming the Matlab code.

References
[1] T. Suckow, P. Groche, Evaluation of Cold Roll Forming Strategies for the Production of a High-Strength Aluminum Hat Profile, Key Eng. Mater. 926 (2022) 690-699. https://doi.org/10.4028/p-y5090o
[2] S. Lee, J. Lee, J. Song, J. Park, S. Choi, W. Noh, G. Kim, Fracture simulation of cold roll forming process for aluminum 7075-T6 automotive bumper beam using GISSMO damage model, Procedia Manuf. 15 (2018) 751-758. https://doi.org/10.1016/j.promfg.2018.07.314
[3] T. Suckow, J. Schroeder, P. Groche, Roll forming of a high strength AA7075 aluminum tube, Product. Eng. 15 (2021) 573-586. https://doi.org/10.1007/s11740-021-01046-2
[4] K. Sweeney, U. Grunewald, The application of roll forming for automotive structural parts, J. Mater. Process. Technol. 132 (2003) 9-15. https://doi.org/10.1016/S0924-0136(02)00193-0
[5] O. Röcker, Untersuchungen zur Anwendung hoch- und höchstfester Stähle für walzprofilierte Fahrzeugstrukturkomponenten, PhD Thesis, Technische Universität Berlin, 2008.
[6] K. Mäntyjärvi, M. Merklein, J. Karjaleinen, UHS Steel Formability in Flexible Roll Forming, Key Eng. Mater. 410 (2009) 661-668. http://doi.org/10.4028/www.scientific.net/KEM.410-411.661
[7] O.M. Badr, B. Rolfe, P.D. Hodgson, M. Weiss, Forming of high strength titanium sheet at room temperature, Mater. Des. 66 (2015) 618-626. http://doi.org/10.1016/j.matdes.2014.03.008
[8] A.D. Deole, M.R. Barnett, M. Weiss, The numerical prediction of ductile fracture of martensitic steel in roll forming, Int. J. Solid. Struct. 144-145 (2018) 20-31. https://doi.org/10.1016/j.ijsolstr.2018.04.011
[9] H. Talebi-Ghadikolaee, H.M. Naeini, M.J. Mirnia, M.A. Mirnia, M.A. Mirzai, S. Alexandrov, M.S. Zeinali, Modeling of ductile damage evolution in roll forming of U-channel sections, J. Mater. Process. Technol. 283 (2020) 116690. http://doi.org/10.1016/j.jmatprotec.2020.116690
[10] T.S. Cao, Models for ductile damage and fracture prediction in cold bulk metal forming processes: a review, Int. J. Mater. Form. 10 (2017) 139-171. https://doi.org/10.1007/s12289-015-1262-7
[11] A.E. Tekkaya, O.-O. Bouchard, S. Bruschi, C.C. Tasan, Damage in metal forming, CIRP Annals. 69 (2020) 600-623. https://doi.org/10.1016/j.cirp.2020.05.005
[12] Y. Lou, S. Lim, K. Pack, New ductile fracture criterion for prediction of fracture forming limit diagrams of sheet metals, Int. J. Solid. Struct. 49 (2012) 3605-3615. https://doi.org/10.1016/j.ijsolstr.2012.02.016
[13] Y. Bai, T. Wierzbicki, A new model of metal plasticity and fracture with pressure and Lode dependence, Int. J. Plast. 24 (2008) 1071-1096. https://doi.org/10.1016/j.ijplas.2007.09.004
[14] Y. Bai, T. Wierzbicki, Application of extended Mohr-Coulomb criterion to ductile fracture, Int. J. Fract. 161 (2010) 1-20. https://doi.org/10.1007/s10704-009-9422-8

[15] H. Wang, Y. Yan, F. Jia, F. Han, Investigations of fracture on DP980 steel sheet in roll forming process, J. Manuf. Process. 22 (2016) 177-184. https://doi.org/10.1016/j.jmapro.2016.03.008
[16] Y. Lou, H. Huh, Prediction of ductile fracture for advanced high strength steel with a new criterion: Experiments and simulation, J. Mater. Process. Technol. 213 (2013) 1284-1302. https://doi.org/10.1016/j.jmatprotec.2013.03.001